JOURNAL OF CATALYSIS 58, 454–469 (1979)

Application of XPS to the Determination of the Size of Supported Particles in a Catalyst—Model Development and Its Application to Describe the Sintering Behavior of a Silica-Supported Pt Film

SHUN C. FUNG

Corporate Research Laboratories, Exxon Research and Engineering Company, Linden, New Jersey 07036

Received August 8, 1978; revised January 19, 1979

A general expression relating the observed XPS intensity ratio of the dispersed phase to the carrier of a catalyst with the size of the dispersed particles has been derived. The shape of the supported particles dictates the type of functional relationship which exists between the observed XPS intensity ratio and the size of the supported particles. This functional relationship has been derived for spherical, hemispherical, and cubic particles. The chemical nature of the catalyst is expressed as a parameter, $\lambda_c(E)$, describing the mean free path for inelastic scattering of the dispersed-phase photoelectrons in the supported particles. A special case can be generated from this general expression to account for a linear relationship of the loading of the dispersed phase with the observed XPS dispersed phase/carrier intensity ratio provided that there is no maldistribution of the supported particles on the surface of the carrier. The derived expression is utilized successfully to describe the sintering behavior of a monoatomic Pt film on a silica substrate under hydrogen.

INTRODUCTION

In order to obtain meaningful comparisons of the activities of supported metal catalysts, it is necessary to know the states of dispersion of the metal particles. Selective gas-adsorption and X-ray diffraction are the most convenient techniques employed in the determination of the size of supported metal particles. However, the former is applicable only for supported transition-metal catalysts and the latter is generally insensitive to particle size below 5 nm. It is desirable to develop a technique which can be applied to any catalyst (e.g., supported metal-oxide or supported metal-sulfide) for particle size determination of the supported phase. X-Ray photoelectron spectroscopy (XPS) appears to be the ideal candidate for this application since it analyzes the near-surface layers of a solid and because every element, with the exception of hydrogen, is susceptible to this technique. However, due to incomplete knowledge of the quantitative basis which relates the spectral intensity to the size and shape of supported particles, the full potential of XPS in particle size determination has not been realized.

Thus, previous attempts in relating XPS dispersed phase/carrier intensity ratio to the size of supported particles have in general not been fruitful. Brinein *et al.* (*1*) correlated XPS peak area ratio (Rh3d/Cls) with metal crystallite size (from X-ray diffraction measurements) for ~12% Rh/carbon catalysts of varying metal dispersion. The large metal crystallite size samples were obtained by hydrogen reduc-

0021-9517/79/090454-16$02.00/0

tion at 400 to 700°C. Significant gasification of the carbon support catalyzed by the rhodium particles was reported by Tomita and Tamai (*2*) at these high temperatures, and as a consequence the rhodium concentration would be well over 12%. This resulted in overestimations of the XPS intensity ratio for these agglomerated catalysts. Scharpen (*3*) attempted to correlate XPS peak area ratios Pt4f/Si2p with total hydrogen adsorption for Pt/SiO_2 catalysts with varying metal loading. Nevertheless, it will be shown later that the functional relationship relating the XPS intensity ratio to the particle size of a supported catalyst differs significantly from that describing the adsorption of hydrogen. Therefore, the correlation failed to accommodate all the experimental data. A recent paper by Angenine *et al.* (*4*) tried to correlate XPS intensity ratio of Pt/SiO_2 with Pt particle size obtained by hydrogen adsorption in the limit that the particle size of Pt $\gg \lambda_{Pt}$, the mean free path of Pt 4f electrons for inelastic scattering, which under their experimental conditions was about 15 Å. Hence, only those samples with Pt particle size greater than 45 Å were suitable for analysis. In addition their correlation was applicable only to cubic particles. In all the references cited, there were no provisions to extract metal particle size from the observed XPS metal/carrier intensity ratio.

In this paper I derive a general expression relating the observed XPS dispersed phase/carrier intensity ratio to the particle size of the supported phase for various particle shapes, i.e., spherical, hemispherical, and cubic. The basic principle can also be applied to disk-shape or raft-like particles. This expression allows one to predict the size of the supported particles from the observed XPS intensity ratio. A special case can be generated from this general expression to account for a linear relationship of the dispersed phase loading with the observed XPS intensity ratio. In addition, the derived expression is utilized successfully to describe the sintering behavior of a monoatomic Pt film on a silica substrate under hydrogen.

EXPERIMENTAL METHODS

The γ-Al_2O_3-supported tungsten catalysts were prepared by impregnating γ-Al_2O_3 with ammonium meta-tungstate solution of the appropriate concentrations to yield, upon calcination, the following catalysts with WO_3 loadings of 1.9, 3.9, 6.5, 9.1, 10, 13.8, and 20%. The catalysts were dried in air at 110–120°C for 16 hr. After drying, a portion of each of the above samples was calcined in air at 500°C for 16 hr. The γ-Al_2O_3, with a BET area of 175 m^2/g, was obtained from Engelhard Industries, Inc., Newark, N.J. as $\{\frac{1}{16}''\}$ cylinders. They were crushed and ground to fine powder before catalyst preparation.

A silica-supported Pt sample was obtained first by depositing a silica layer of 75 nm onto a 5×10^{-3} cm thick stainless-steel foil. Platinum was then evaporated at 10^{-6} Torr onto the silica support from a spectrographically pure Pt wire mounted on a tungsten filament. This produced a Pt film approximately one atom thick.

XPS measurements were obtained on the pressed powder samples of γ-Al_2O_3-supported tungsten catalysts without any sample treatment. The powder samples were pressed onto a 80×80-mesh Ag screen of 0.4×1.1 cm. In contrast the supported Pt sample was reduced under hydrogen before each XPS measurement. The Pt sample was cut into a 2-cm strip and mounted onto a sample holder which was fastened to a bellow arrangement and was readily extended into the electron-spectrometer. The sample holder was contained in a reaction vessel which could be isolated from the spectrometer. Hydrogen treatment of the sample was carried out in the reaction chamber at the following temperature, 150, 300, 500, 600, and 700°C

with a 20% hydrogen/helium mixture under flow conditions for 1 hr. After each reduction period the sample was cooled under the gas mixture and evacuated before inserting into the spectrometer. XPS measurements were performed in a Model 200A AEI Scientific Instruments Spectrometer with an aluminum anode. The intensity ratios R_d were obtained as the ratios of the corresponding peak areas.

RESULTS AND DISCUSSION

Basis of Size Determination of Supported Particles by XPS

In analyzing the intensity of a XPS signal, it is necessary to take into account that the mean free path of kilovolt X rays in matter is several orders of magnitude greater than that of the photoejected electrons. Thus, the X-ray beam is essentially unattenuated over the range of surface thickness from which photoelectrons emerge without any energy loss due to inelastic collisions. Therefore, the probing depth of XPS is determined by the mean free path of the photoelectron which ranges from 0.4 to 3 nm when the energy of the photoelectron is 100 to 1500 eV (*5*). In general the thickness of a carrier particle, b, is much greater than the mean free path, λ_s, for inelastic scattering of a photoelectron in carrier S. This condition is still satisfied even for a porous carrier such as Al_2O_3. The wall thickness of an average pore in an alumina particle is in the order of 10 nm, since this is the average size of the Al_2O_3 crystallites from which the porous structure is constructed. Therefore, the XPS intensity ratio, R_d, between two particular photoelectron lines which are associated with the dispersed phase and the carrier, respectively, is a function of the number of dispersed particles on the external surfaces (not within the pores) of the alumina particles. The use of R_d instead of the integrated intensities of each photoelectron line in the quantification of XPS data frees one from dealing with problems associated with nonreproducibility of the geometry and morphology of a series of samples, since R_d is independent of the physical nature of the samples. The number of supported particles per unit of external surface area of a carrier particle depends on the specific metal loading, the specific surface area of the carrier, and the size and shape of the supported particles as well as their distribution on the carrier surface. Attenuation of the intensity of the carrier photoelectron line by the supported particles can be neglected when the surface area of the carrier is high and the metal loading is relatively low, because under these conditions the surface coverage of the carrier is low. If the effect of carbon contamination overlayer is neglected and with a detector arrangement which collects only the photoelectrons emerging from the sample surface at 90°, the XPS intensity ratio of dispersed phase/carrier, R_d, can be shown to have the following functional relationship with the shape and the average size of supported particles (see Appendix A on detailed mathematical analysis).

$$R_d = k \cdot \frac{W}{DSd} \frac{\lambda_c(E) H_c}{\lambda_s(E') H_s} \Psi(d, \lambda_c(E)) \quad (1)$$

where k is a proportional constant describing the distribution of the supported particles on the surface of the carrier, W is the weight of the dispersed phase/g of catalyst, D is the density of the dispersed phase, S is the surface area of the carrier/g of catalyst, $\lambda_c(E)$ is the mean free path of inelastic scattering of the dispersed phase photoelectrons of energy E in the supported particles, $\lambda_s(E')$ is the mean free path of inelastic scattering of the carrier photoelectrons of energy E' in the carrier, H_c is the spectroscopic constant of the dispersed phase, H_s is the spectroscopic constant of the carrier, d is a characteristic dimension of the supported particles; the diameter of a spherical or hemispherical particle, the edge

TABLE 1

Dependency of Standardized XPS Intensity Ratio on the Shape and Size of the Supported Particles—Reference to 1-nm Particles

Particle size (nm)	Standardized XPS intensity ratio N					
	Sphere $\lambda_e(E)$		Hemisphere $\lambda_e(E)$		Cube $\lambda_e(E)$	
	1 nm	1.5 nm	1 nm	1.5 nm	1 nm	1.5 nm
1	1	1	1	1	1	1
2	0.746	0.809	0.847	0.891	0.684	0.757
3	0.581	0.668	0.727	0.799	0.501	0.592
4	0.470	0.564	0.631	0.720	0.388	0.478
5	0.392	0.484	0.555	0.653	0.314	0.396
6	0.334	0.421	0.492	0.596	0.263	0.336
8	0.257	0.332	0.398	0.502	0.198	0.256
10	0.208	0.273	0.332	0.431	0.158	0.206
12	0.174	0.230	0.283	0.376	0.132	0.171
14	0.150	0.199	0.246	0.332	0.113	0.147

of a cubic particle, and the thickness of a disk or raft, $\Psi(d,\lambda_e(E))$ is the shape factor and is a function of the shape and average size of the supported particles, and $\lambda_e(E)$. Its explicit forms for various particle shapes are as follows:

Supported spherical particles

$$\Psi_s(d, \lambda_e(E)) = \frac{3}{2}\left\{1 - \frac{2\lambda_e^2(E)}{d^2} \times [1 - \exp(-d/\lambda_e(E))] + \frac{2\lambda_e(E)}{d}\exp(-d/\lambda_e(E))\right\} \quad (2)$$

Supported hemispherical particles

$$\Psi_{HS}(d, \lambda_e(E)) = 3\left\{1 - \frac{8\lambda_e^2(E)}{d^2} \times [1 - \exp(-d/2\lambda_e(E))] + \frac{4\lambda_e(E)}{d}\exp(-d/2\lambda_e(E))\right\} \quad (3)$$

Supported cubic particles, or disks or rafts

$$\Psi_c(d,\lambda_e(E)) = 1 - \exp(-d/\lambda_e(E)) \quad (4)$$

Equation (1) describes how the XPS intensity ratio varies with the particle size d of the supported particles, the loading of the dispersed phase, and the surface area of the carrier. If we study a series of catalysts with various dispersed phase loading and examine the intensity ratio of two particular photoelectron lines associated with the dispersed phase and the carrier, respectively, R_d will vary linearly with the loading of the dispersed phase provided the size of the supported particles does not vary and there is no change in the shape of the catalyst particles. An even more important parameter is the distribution constant k which is assumed to maintain a constant value in spite of the variation in the dispersed phase loading. More often k depends strongly on catalyst preparation. The inefficient use of all the available surface area of the carrier, especially in highly porous materials with large variation in pore size, results in drastic change in the k values. The preferential deposition of the dispersed phase on the external surface of the carrier particles results in a large k whereas small k is obtained when the dispersed phase concentrates in the porous structure of the carrier. Variation in R_d for a series of catalysts with no change in the size of the supported particles provides information about the distribution

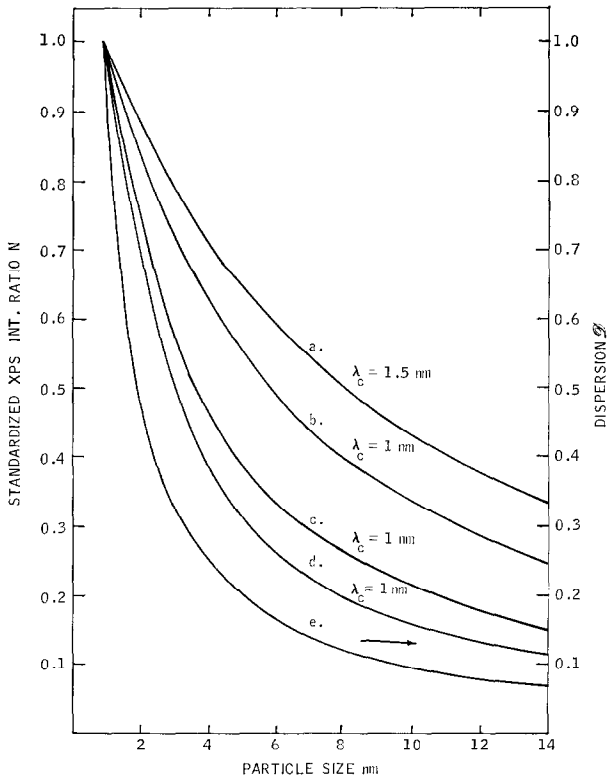

FIG. 1. Dependency of the standardized XPS intensity ratio on the shape and size of the supported particles. Reference state 1-nm particle (a) and (b) hemispherical, (c) spherical, (d) cubic particles, (e) dispersion curve.

of the dispersed phase on the carrier surface. The constants H_c and H_s remain constant for all samples since they are studied under the same spectrometer conditions. It is not practical to employ Eq. (1) to calculate the size of the supported particles from the observed R_d since the magnitude of k can be obtained experimentally only by examining the dependency of R_d with the loading of the dispersed phase and at the same time keeping the particle size constant. It is more useful to obtain a relationship which describes the change in R_d with the size of the supported particles independent of the nature of the catalyst. Equation (5) describes the decrease in R_d, which has been normalized with respect to the loading of the dispersed phase and the surface area of the carrier, from a standard catalyst due to increase in the size of the supported particles.

$$N = \frac{R_d W_0 S}{R_{d_0} W S_0} = \frac{d_0}{d} \frac{\Psi(d, \lambda_c(E))}{\Psi_0(d_0, \lambda_c(E))}$$

$$\text{when} \quad k = k_0 \quad \text{and} \quad d_0 = 1 \text{ nm} \qquad (5)$$

The selection of the 1-nm particle size as the reference state has a practical significance since the dispersion of such a catalyst is close to 100%. The only parameter which affects the relationship between N and d is $\lambda_c(E)$ which is a function of the catalyst material and the energy of the photoelectrons. It is easy to show that N, the standardized XPS intensity ratio, decreases from unity with an increase in the size of the supported particles. With $\lambda_c(E)$ as the parameter one can construct a set of curves describing the dependency of N on the size of the supported particles.

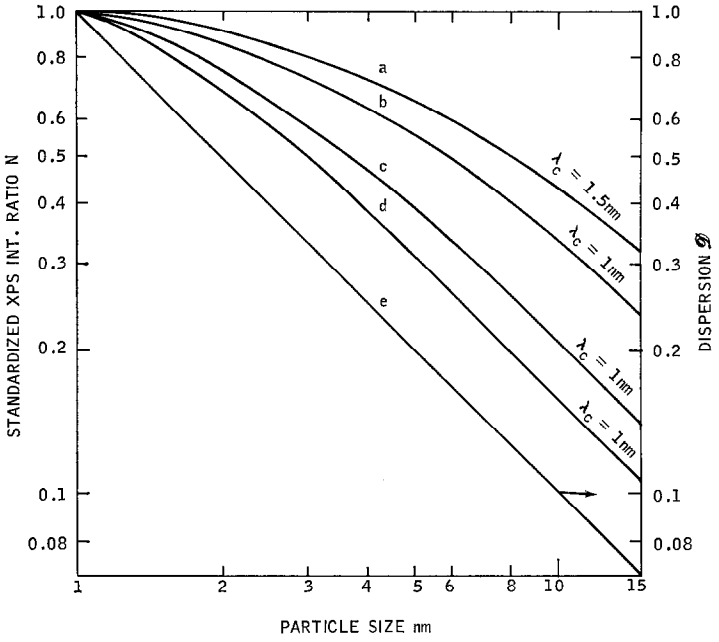

FIG. 2. Log–log plots of the dependency of the standardized XPS intensity ratio on the shape and size of the supported particles. Reference state 1-nm particle (a) and (b) hemispherical, (c) spherical, (d) cubic particles, (e) dispersion curve.

This relationship is applicable for supported metal, metal-oxide, or metal-sulfide particles and is especially useful for the latter two types of catalysts, since particle size determination by gas adsorption is generally not suitable with these catalysts and they are generally amorphous to X-ray diffraction. The calculated N values as a function of d with $\lambda_c(E) = 1$ and 1.5 nm are shown in Table 1 and Fig. 1.

The relationship of catalyst dispersion and the size of the supported particle is also illustrated in Fig. 1. Practically all the atoms in a 1-nm particle are exposed and the catalyst dispersion corresponds to unity. It is easily shown that catalyst dispersion, $\mathfrak{D}$, is an inverse function of the size of the supported particle and is independent of the particle shape for the particle shapes considered here. This inverse relationship is represented by the straight line in Fig. 2 which is constructed from Fig. 1 with logarithmic coordinates. A slope of -1 indicates the inverse relationship between $\mathfrak{D}$ and d. Figure 2 clearly illustrates the different functional relationship of dispersion, $\mathfrak{D}$, and of the standardized XPS intensity ratio, N, with the size of the supported particles. The standardized XPS intensity ratio, N, has less dependency on particle size as compared to the dispersion of the catalyst. This is due to the fact that gas adsorption, which is generally used to obtain metal dispersion, measures only the surface atoms and results in a surface average size. On the other hand, a volume average size is obtained by X-ray line broadening. X-Ray photoelectron spectroscopy gives something between a surface and volume average size, since the surface atoms and atoms below the surface contribute significantly to the intensity of an XPS signal.

Returning to Fig. 2, one notices that in the limit of very large particles with $d \gg \lambda_c(E)$, N is inversely proportion to d. In particular, Curve (d) of the cubic particles develops into a straight line with a

slope of -1 when $d \geq 3\lambda_e(E)$. This suggests that Curve (d) would coincide with Curve (e) if $\lambda_e(E)$ would have a value of less than 0.3 nm. Substantially larger particles with $d \geq 6\lambda_e(E)$ and $d \geq 10\lambda_e(E)$ are required to attain the inverse relationship between N and d when the particles are spherical and hemispherical, respectively. Therefore, in the limit of large particles, XPS measurements result in a surface average size.

In the case of very small particles with $d \ll \lambda_e(E)$, the standardized XPS intensity ratio, N, does not depend on the size of the supported particles and therefore serves no useful purpose in particle size determination. For simplicity, we choose supported cubic particles as an illustration. The shape factor of a cubic particle represented by Eq. (4) is reduced to $d/\lambda_e(E)$ when d is much smaller than $\lambda_e(E)$. With this shape factor substituted in Eq. (5), we obtain a constant value for N at any particle size within the limit of $d \ll \lambda_e(E)$. The physical significance of this resides on the fact that atoms on the surface of the particles as well as those within contribute *equally* to the XPS signal. In other words, photoelectrons emitted within the particles are essentially unattenuated due to the large $\lambda_e(E)$. Fortunately, values of $\lambda_e(E)$ do not greatly exceed the particle size range of practical interest and therefore, particle size determination is possible by XPS measurements.

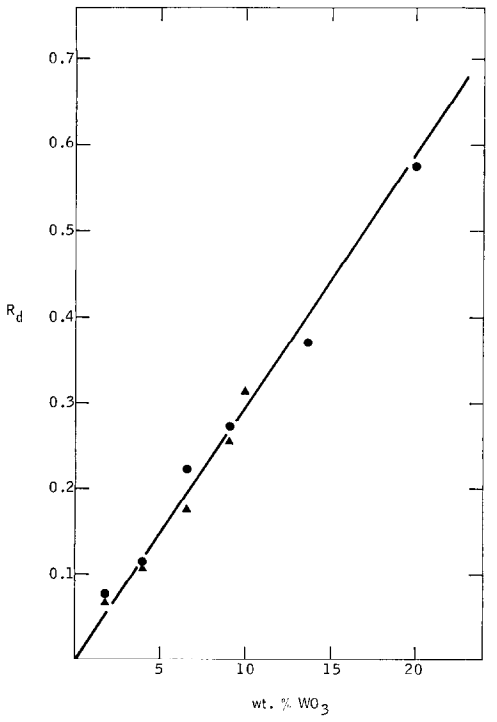

FIG. 3. Dependency of R_d on the loading of tungsten in γ-Al_2O_3 supported tungsten catalysts: ●, impregnated and dried; ▲, calcined at 500°C.

TABLE 2

XPS Intensity Ratio Pt4f/Si2p of a Silica-Supported Monoatomic Pt Film Sintered under Hydrogen

Reduction temperature (°C)	Pt4f/Si2p (R_d)	Std. intensity ratio (N)
—	1.735	1
150	1.457	0.840
300	1.062	0.612
500	0.915	0.527
600	0.821	0.473
700	0.701	0.404

The Linear Relationship between R_d and the Supported Phase Loading—WO_3/γ-Al_2O_3

The intensity ratio W4f/Al2s is calculated from the area of the W4f peaks (spin doublet) and the area of the Al2s peak. This ratio increases linearly with the loading of WO_3 as is shown in Fig. 3. The impregnated and the calcined samples fall onto the same straight line. This indicates that there is no difference between these two groups of catalysts and the catalysts within each group, in the shape and the average size of their tungsten particles as well as in the distribution of the tungsten particles on the surface of γ-Al_2O_3. It is not surprising that the special requirements in Eq. (1) for the establishment of a linear relationship between R_d and W are satisfied by these WO_3/γ-Al_2O_3 catalysts based on

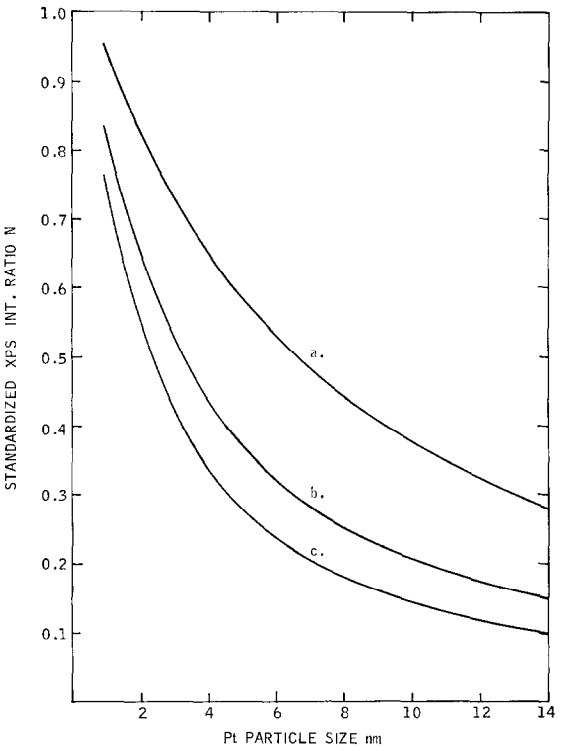

FIG. 4. Dependence of the standardized XPS intensity ratio on the shape and size of the supported Pt particles. Reference state monoatomic Pt film $d_0 = 0.247$ nm (a) hemispherical, (b) spherical, (c) cubic particles

the chemical property of supported WO_3. Biloen and Pott (*6*) in their XPS studies of the reducibility of WO_3 and supported WO_3 reported that γ-Al_2O_3 stabilized WO_3 from being reduced to lower valence states in hydrogen up to 550°C. A few years later Ng and Hercules (*7*) investigated nickel-tungsten catalysts supported on γ-alumina after reduction and sulfiding and arrived at a similar conclusion. They postulated that the stability of WO_3 in hydrogen was due to the formation of a surface complex between WO_3 and γ-Al_2O_3. This is in agreement with the data presented in Fig. 3 which indicate that up to a maximum coverage of 80%, the deposited WO_3 does not agglomerate and is dispersed on the surface of Al_2O_3 in monolayer thickness. This maximum coverage is calculated for 175 m^2/g γ-Al_2O_3 using an O^{-2} ion density of 9.1×10^{18} ions/m^2 for the (110) surface (*8*) and assuming one W ion bonded to two O^{-2} ions on the γ-Al_2O_3 surface.

At this maximum coverage the attenuation of the intensity of the Al2s photoelectrons by the WO_3 overlayer is estimated to be 8%. Hence the proposed model in neglecting the attenuation effect by the dispersed phase on the high surface area carrier is justified. The maximum attenuation is calculated from the reported monolayer thickness of WO_3 (*9*) and the mean free path for inelastic scattering of Al2s photoelectrons in WO_3. The latter is assumed to have the same value of the mean free path for inelastic scattering of W4f photoelectrons in WO_3 reported in (*9*), since the kinetic energy of Al2s photoelectrons is lower by about 90 eV than the 1450 eV reported for W4f.

TABLE 3

Sintering of a Silica-Supported Monoatomic Pt Film to Particles of Various Shapes

Reduction temperature (°C)	Std. intensity ratio (N)	Characteristic dimension of the Pt particles (nm)		
		Hemispherical	Spherical	Cubic
150	0.840	2.0	1.0	0.8
300	0.612	4.7	2.3	1.7
500	0.527	6.2	3.1	2.2
600	0.473	7.4	3.7	2.6
700	0.404	9.2	4.6	3.2

Determination of Pt Particle Size by XPS Intensity Ratio

The intensity ratio Pt4f/Si2p is calculated from the area of the Pt4f peaks (spin doublet) and the area of the Si2p peaks. Table 2 lists the intensity ratio Pt4f/Si2p obtained at each sintering temperature. Their values standardized with respect to that of the fresh sample are shown in Table 2. Sintering of the monoatomic Pt film under hydrogen obviously decreases the intensity ratio Pt4f/Si2p.

The working curves in Fig. 1 describing the relationship between the standardized intensity ratio, N, and the size of the supported particles are derived for low coverage of the carrier by the dispersed phase and with reference to 1-nm particles and therefore cannot be directly applied to describe the sintering behavior of a monoatomic Pt film. A new set of working curves are constructed in Fig. 4, by employing monoatomic Pt film as the reference state and taking into account the change in surface coverage of the silica by the sintered Pt particles. The derived functional relationships for spherical, hemispherical, and cubic particles are detailed in Appendix B. The exact value of the mean free path for inelastic scattering of the 4f platinum photoelectrons has not been reported. However, a reasonable value of about 1.5 nm can be obtained from the universal curve (*5*). From the experimental N values, the size of the Pt particle at each sintering temperature was determined from the working curves in Fig. 4 and are listed in Table 3. Interestingly, the decrease in the standardized intensity ratio, N, at each sintering temperature is the same for hemispherical and spherical particles when the former have a characteristic dimension twice that of the latter.

A uniform carbon contamination on the surface of the sample has little effect on the ratio Pt 4f/Si2p since the carbon layer has the same degree of attenuation on the 4f platinum and 2p silica photoelectrons, because there is little difference in their mean free path in carbon (see Appendix B). The error in determining the initial thickness of the Pt film has only a minor influence on the N values of the working curves, since N is proportional to $d/[1 - \exp(-d/\lambda_e(E))]$, where d is the thickness of the Pt film in the fresh sample. The doubling of the Pt film thickness from monoatomic to diatomic reduces the N values by less than 10% at any given Pt particle size.

The sintering behavior of this silica-supported Pt film under hydrogen has been determined by transmission electron microscope (TEM) (*10*). The Pt particles were circular in shape. In regard to the three-dimensional nature of the Pt particles, TEM could not distinguish between sphere and hemisphere. Figure 5 compares the growth of the Pt particles as a function of sintering temperature determined by the above two

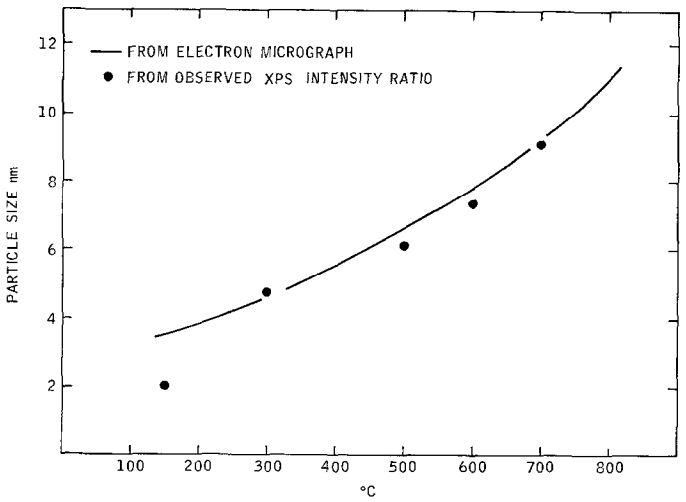

FIG. 5. Sintering behavior of a monoatomic Pt film/silica under hydrogen.

techniques. With the exception of the 150°C reduction, the Pt particle sizes determined by the two techniques are in good agreement when the Pt particles are assumed to be hemispherical. The substantially smaller Pt particle size determined by XPS after 150°C reduction indicated that at this temperature the Pt particles had not attained the shape of a hemisphere but rather they were closer to disk-like particles with a thickness of 2 nm. Substantially underestimated Pt particle size is obtained at each sintering temperature when the particles are assumed to be cubic or spherical as is indicated in Table 3. In order to obtain particle size data of the cubic and spherical particles in agreement with those obtained by TEM, λ_{Pt} for the 4f platinum photoelectron would have to be unreasonably large.

The above model is based on a single parameter distribution function of particle sizes in order to simplify the mathematics. Deviation from the assumed uniform particle size, as is more than often encountered in a practical catalyst, introduces an error of about 10% in an overestimation of the size of Pt particles as compared to that obtained by TEM (see Appendix C). Hence the validity of the proposed model has been demonstrated and at the same time information about the shape of the supported Pt particles is obtained.

CONCLUSION

As a result of a detailed analysis of the effect of the size and shape of supported particles on the XPS dispersed phase/carrier intensity ratio, the average size of Pt particles supported on silica at each sintering temperature has been determined directly from XPS measurements. These particle sizes are in good agreement with those obtained from TEM. A special case is generated from the derived expression and provides a good description on the variation of the XPS intensity ratio W 4f/Al2s with the loading of WO_3 on γ-Al_2O_3.

Limitations do exist in using this model for particle size determination. The most important assumption is that the distribution constant k remains unchanged in spite of the variations in the dispersed phase loading and catalyst treatment conditions. The inefficient use of all the available surface area of the carrier, especially in highly porous materials with large variation in pore size, results in drastic change in the

k value. Without any knowledge about the exact value of k for each catalyst, particle size determination of the supported particles is not possible by the derived expression in Eq. (5). On the other hand, if the supported particles of a series of catalysts are found to have the same size and shape by an independent technique, the relative magnitudes of the distribution constant k for these catalysts can be obtained from Eq. (1), since k is proportional to the observed XPS intensity ratio of dispersed phase/carrier.

In addition to the requirement of a constant k value, at least a calibration-sample is needed to establish the reference state. In other words, the size of the supported particles in this calibrated sample has to be determined by an independent technique. From this, R_{d_0} of a chosen standard state can be calculated for various particle shapes using Eq. (5). Once this is established, particle size of the supported particles (of a particular shape) in the rest of the samples can be determined by the use of the working curves in Figs. 1 or 4 according to the stated conditions (see Appendixes A and B). In principle, the exact particle shape can be determined if another particle size which differs from that of the standard sample is available by an independent technique. The closest agreement of the particle size between the actual measured value (by the independent technique) and one of the calculated values obtained for various particle shapes (by the observed R_d) indicates that the assumed shape is correct. However, even without any knowledge about the particle shape, one can obtain an indication of the trend of the size of the supported particles in a series of catalysts by XPS measurements through the use of Eq. (5).

In general, the use of XPS measurements for particle size determination of the supported particles is more complex than the gas adsorption and X-ray line broadening. Certain unique conditions (such as constant k values and stable particle shape) have to be satisfied before meaningful particle size informations can be obtained. Nevertheless, because of the success in establishing the quantitative basis for XPS measurements in the determination of the size of supported particles, photoelectron spectroscopy is a promising technique for particle size determination especially when gas adsorption and X-ray line broadening fail to yield meaningful data.

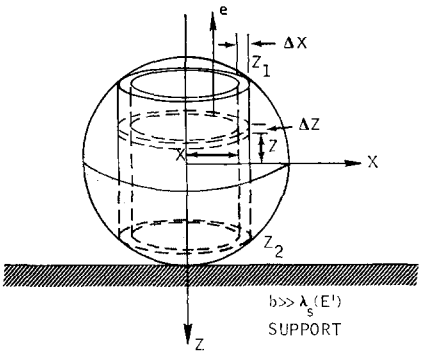

FIG. 6. Cross-sectional view of a spherical particle on the carrier surface.

APPENDIX

A. Dependency of XPS Dispersed Phase/Carrier Intensity Ratio on the Size of Supported Spherical Particles

The precise form of the functional relationship between the XPS dispersed phase/carrier intensity ratio and the size of supported particles depends on the shape of the latter. As an illustration, a detailed analysis of the functional relationship is presented for supported spherical particles. However, functional relationships for particles other than spherical in shape are easily obtained if one follows the procedures outlined for the spherical particles.

It is easy to show that the observed intensity of an XPS signal for a given subshell of a given element from a volume element dv within a solid at a distant z below the surface of the solid is:

$$dI = H \cdot F \cdot G \exp(-z/\lambda_m(E))dv \quad \text{(A1)}$$

where F is the X-ray flux, G is a constant which depends on the physical nature of the sample surface, and H is the spectroscopic constant which contains information such as the concentration of an element in terms of atoms per unit volume in the solid, the sensitivity of the spectrometer to the ejected photoelectrons as a function of photoelectron energy, and the cross-sections of photoelectrons as well as their angular distribution.

In applying Eq. (A1) to a spherical particle of radius a, the most critical step is the designation of the volume element dv. The volume element is chosen in such a manner that material within this volume element is at the same distance away from the surface of the spherical particle. Such a volume element is depicted in Fig. 6 as the ring element $2\pi x dz dx$. Integration with respect to z from z_2 to z_1 yields the elemental shell volume. The second integration with respect to x from zero to a generates the sphere. It is assumed that there are n particles of radius a within the sampling area A, from which electrons emerge and are collected by the spectrometer. Furthermore the thickness, b, of the carrier is assumed to be much greater than λ_s, the mean free path for inelastic scattering of a photoelectron in the carrier S. With a detector arrangement which collects only the photoelectrons emerging from the surface of the sample at 90° as shown in Fig. 6, the intensity of a particular photoelectron associated only with the supported particles can be calculated by applying Eq. (A1) to one of these particles and multiplying it by n as is shown in Eq. (A2).

$$I_{c,n_1l_1} = n \int_0^a \int_{z_2}^{z_1} H_c \cdot F \cdot G 2\pi x \times \exp(-(z - z_1)/\lambda_c(E)) dz dx \quad \text{(A2)}$$

where

$$z_1 = -(a^2 - x^2)^{\frac{1}{2}} \quad \text{(A3)}$$

$$z_2 = +(a^2 - x^2)^{\frac{1}{2}} \quad \text{(A4)}$$

and subscript c refers to the dispersed phase. Equation (A2) is integrated to give:

$$I_{c,n_1l_1} = n\lambda_c(E) H_c \cdot F \cdot G\pi a^2 \left\{1 - \frac{\lambda_c^2(E)}{2a^2} \times [1 - \exp(-2a/\lambda_c(E))] + \frac{\lambda_c(E)}{a} \exp(-2a/\lambda_c(E))\right\} \quad \text{(A5)}$$

Let f be the fraction of the carrier surface which is covered by the particles. The photoelectrons emerging from this portion of the carrier are further attenuated by the particles. Using the ring element $2\pi x dz dx$ as the volume element for the carrier and noting the proper limits on each integral, the XPS intensity of a particular photoelectron from this portion of the carrier is:

$$\hat{I}_{s,n_2l_2} = n \int_0^a \int_a^\infty H_s \cdot F \cdot G 2\pi x \times \exp(-(z - a)/\lambda_s(E')) \times \exp(-(z_2 - z_1)/\lambda_c(E')) dz dx \quad \text{(A6)}$$

The last exponential term in Eq. (A6) is the attenuation that the photoelectrons from the carrier has to suffer when they are passing through the particles. Equation (A6) is integrated to give:

$$\hat{I}_{s,n_2l_2} = fA\lambda_s(E') H_s \cdot F \cdot G \cdot 2 \left[\frac{\lambda_c^2(E')}{4a^2} - \frac{\lambda_c(E')}{2a} \exp(-2a/\lambda_c(E')) - \frac{\lambda_c^2(E')}{4a^2} \exp(-2a/\lambda_c(E'))\right] \quad \text{(A7)}$$

and

$$f = \frac{n \cdot \pi a^2}{A}. \quad \text{(A8)}$$

The contribution to the XPS intensity from the portion of carrier which is not

covered is simply $(1-f)A\cdot M_s\cdot F\cdot G$. Hence,

$$I_{s,n_2l_2} = A\lambda_s(E')H_s\cdot F\cdot G \times \left\{1 - f\left[1 - \frac{\lambda_c^2(E')}{2a^2} + \frac{\lambda_c(E')}{a}\exp(-2a/\lambda_c(E')) + \frac{\lambda_c^2(E')}{2a^2}\exp(-2a/\lambda_c(E'))\right]\right\}. \quad \text{(A9)}$$

In general, the surface area of the carrier is very high and for low loading of the dispersed phase, f tends to be very small and Eq. (A9) becomes

$$I_{s,n_2l_2} = A\lambda_s(E')H_s\cdot F\cdot G \quad \text{(A10)}$$

the intensity ratio of the dispersed phase to the carrier for the two distinct photoelectron lines is calculated from Eqs. (A5) and (A10)

$$R_d = \frac{I_{c,n_1l_1}}{I_{s,n_2l_2}} = \frac{n\pi a^2}{A}\cdot\frac{\lambda_c(E)H_c}{\lambda_s(E')H_s} \times \left\{1 - \frac{\lambda_c^2(E)}{2a^2}[1 - \exp(-2a/\lambda_c(E))] + \frac{\lambda_c(E)}{a}\exp(-2a/\lambda_c(E))\right\}. \quad \text{(A11)}$$

Experimentally, I_c and I_s are obtained from the same sample, therefore, R_d is independent of X-ray flux, F, and the physical nature of the sample surface, G. In addition n is related to the size of the particles by the following equation:

$$n\alpha A\cdot n_s = k\cdot A\cdot W/(D\tfrac{4}{3}\pi a^3 S) \quad \text{(A12)}$$

Where k is a proportional constant related to the distribution of the supported particles on the surface of the carrier, n_s is the number of supported particles/unit area of the carrier, W is the weight of the dispersed phase/g of catalyst, D is the density of the dispersed phase, and S is the surface area of the carrier/g of catalyst.

From Eqs. (A11) and (A12)

$$R_d = k\cdot\frac{W}{DSd}\cdot\frac{\lambda_c(E)H_c}{\lambda_s(E')H_s}\cdot\frac{3}{2}\left\{1 - \frac{2\lambda_c^2(E)}{d^2}[1 - \exp(-d/\lambda_s(E))] + \frac{2\lambda_c(E)}{d}\exp(-d/\lambda_c(E))\right\} \quad \text{(A13)}$$

or

$$R_d = k\cdot\frac{W}{DSd}\cdot\frac{\lambda_c(E)H_c}{\lambda_s(E')H_s}\Psi_s(d, \lambda_c(E)) \quad \text{(A14)}$$

where

$$\Psi_s(d, \lambda_c(E)) = \frac{3}{2}\left\{1 - \frac{2\lambda_c^2(E)}{d^2} \times [1 - \exp(-d/\lambda_c(E))] + \frac{2\lambda_c(E)}{d}\exp(-d/\lambda_c(E))\right\} \quad \text{(A15)}$$

and $d = 2a$.

B. Application of the Models to Sintering of a Monoatomic Pt Film

No matter what shape the Pt particles attain after sintering under hydrogen, its initial state is a monoatomic film. Hence, the latter is employed as the reference state in the construction of the working curves in Fig. 4. The effective thickness of a monoatomic Pt film is estimated from the unit cell dimension of platinum. Since platinum is a face center cube, there are 4 atoms per unit cell and its unit cell dimension is 0.39231 nm. The effective film thickness $d_0 = [(0.39231)^3/4]^{\frac{1}{3}} = 0.247$ nm. Equation (5) for spherical, hemispherical, and cubic particles become, respectively

$$N_{\text{Sphere}} = \frac{0.247}{d}\frac{\Psi_s(d, \lambda_{Pt}(E))}{\Psi_c(0.247, \lambda_{Pt}(E))} \quad \text{when } k = k_0;\ d_0 = 0.247 \text{ nm} \quad \text{(B1)}$$

$$N_{\text{Hemisphere}} = \frac{0.247}{d} \frac{\Psi_{\text{HS}}(d, \lambda_{\text{Pt}}(E))}{\Psi_{\text{c}}(0.247, \lambda_{\text{Pt}}(E))}$$

when $k = k_0$; $d_0 = 0.247$ nm (B2)

$$N_{\text{Cube}} = \frac{0.247}{d} \frac{\Psi_{\text{c}}(d, \lambda_{\text{Pt}}(E))}{\Psi_{\text{c}}(0.247, \lambda_{\text{Pt}}(E))}$$

when $k = k_0$; $d_0 = 0.247$ nm (B3)

where Ψ_{s}, Ψ_{HS}, and Ψ_{c} functions are expressed as in Eqs. (2), (3), and (4).

However, Eqs. (B1), (B2), and (B3) are obtained with the assumption that there is no change in the Si2p intensity due to the coverage of Pt. As a matter of fact, a significant change in the Si2p intensity definitely occurred with the sintering of the Pt film to individual platinum particles since the Pt coverage f decreased appreciably from unity as the Pt film proceeded to high degree of sintering.

Since

$$N = \frac{\text{Intensity Ratio Pt4f/Si2p when Pt sintered to particle of size } d}{\text{Intensity Ratio Pt4f/Si2p when Pt is a monoatomic film}} \quad \text{(B4)}$$

$$= \frac{I_{\text{Pt}}(d)}{I_{\text{Pt}}(0.247 \text{ nm})} \cdot \frac{I_{\text{Si}}(0.247 \text{ nm})}{I_{\text{Si}}(d)} \quad \text{(B5)}$$

$$= \frac{I_{\text{Pt}}(d)}{I_{\text{Pt}}(0.247 \text{ nm})} \cdot Q \quad \text{(B6)}$$

Hence, the corrected std. XPS intensity ratio N for spherical, hemispherical, and cubic particles can be obtained from Eqs. (B1), (B2), and (B3) by multiplying the corresponding N values with the factor Q at a given Pt particle size. It is easy to show that

$$I_{\text{Si}}(0.247 \text{ nm}) = A \cdot F \cdot G \cdot \lambda_{\text{Si}}(E') H_{\text{Si}} \times \exp(-0.247/\lambda_{\text{Pt}}(E')) \quad \text{(B7)}$$

the exponential factor is the attenuation of the Si2p photoelectron by the Pt film, and $\lambda_{\text{Pt}}(E')$ is the mean free path for inelastic scattering of Si2p photoelectrons in platinum. $I_{\text{Si}}(d)$ for spherical Pt particles is obtained from Eq. (A9).

$$I_{\text{Si}}(d) = A \cdot \lambda_{\text{Si}}(E') H_{\text{Si}} \cdot F \cdot G \times \left\{1 - f\left[1 - \frac{2\lambda_{\text{Pt}}^2(E')}{d^2} + \frac{2\lambda_{\text{Pt}}(E')}{d} \exp(-d/\lambda_{\text{Pt}}(E')) + \frac{2\lambda_{\text{Pt}}^2(E')}{d^2} \exp(-d/\lambda_{\text{Pt}}(E'))\right]\right\} \quad \text{(B8)}$$

From Eqs. (B7) and (B8)

$$Q_{\text{Sphere}} = \frac{\exp(-0.247/\lambda_{\text{Pt}}(E'))}{1 - f\left[1 - \frac{2\lambda_{\text{Pt}}^2(E')}{d^2} + \frac{2\lambda_{\text{Pt}}(E')}{d} \exp(-d/\lambda_{\text{Pt}}(E')) + \frac{2\lambda_{\text{Pt}}^2(E')}{d^2} \exp(-d/\lambda_{\text{Pt}}(E'))\right]} \quad \text{(B9)}$$

and

$$f = \frac{n \cdot \pi a^2}{A} = \frac{(A0.247/\frac{4}{3}\pi a^3) \cdot \pi a^2}{A} \quad \text{(B10)}$$

$$f = \frac{3(0.274)}{4a} \quad \text{(B11)}$$

$\lambda_{Pt}(E') \simeq \lambda_{Pt}(E)$. Since the energy difference between the Si2p and Pt4f photoelectrons is about 30 eV out of an energy range of 1400 eV. Hence, Q can be calculated at any Pt particle size with $\lambda_{Pt}(E)$ as the parameter. The working curve for the supported Pt film is constructed from Eq. (B6) with the proper utilization of Eqs. (B1), (B9), and (B11). In the same manner Q for the hemispherical and cubic particles is shown by Eqs. (B12) and (B14). Their working curves with $\lambda_{Pt}(E) = 1.5$ nm are in Fig. 4.

$$Q_{\text{Hemisphere}} = \frac{\exp(-0.247/\lambda_{Pt}(E'))}{1 - f\left[1 - \frac{8\lambda_{Pt}^2(E')}{d^2} + \frac{4\lambda_{Pt}(E')}{d}\exp(-d/2\lambda_{Pt}(E')) + \frac{8\lambda_{Pt}^2(E')}{d^2}\exp(-d/2\lambda_{Pt}(E'))\right]} \quad \text{(B12)}$$

and

$$f = \frac{3(0.247)}{2a} \quad \text{(B13)}$$

$$Q_{\text{Cube}} = \frac{\exp(-0.247/\lambda_{Pt}(E'))}{1 - f[1 - \exp(-d/\lambda_{Pt}(E'))]} \quad \text{(B14)}$$

and

$$f = \frac{0.247}{d}. \quad \text{(B15)}$$

C. Effect of Particle Size Distribution on the Average Particle Size Obtained by Electron Micrographs and XPS Measurements

The following particle distribution is assumed for 1 g of catalyst with a metal loading of W:

Number of metal particles/ g catalyst	Particle diameter
n_1	d_1
n_2	d_2
—	—
n_n	d_n

for hemispherical particles

$$n_i = \frac{\frac{X_i W}{D}}{\frac{1}{12}\pi d_i^3} \quad \text{(C1)}$$

where X_i is the weight fraction of metal forming particles of d_i. The average particle diameter obtained by electron micrograph is:

$$\bar{d} = \frac{\sum_i n_i d_i^3}{\sum_i n_i d_i^2} \quad \text{(C2)}$$

Substitute Eq. (C1) into Eq. (C2) we obtain

$$\bar{d} = \frac{1}{\sum_i \frac{X_i}{d_i}} \quad \text{(C3)}$$

e.g., TEM indicates the following distribution of Pt particles after the silica-supported

Pt film has been sintered:

40% of the metal in 1 g of the catalyst forming 3-nm particles
20% of the metal in 1 g of the catalyst forming 5-nm particles
30% of the metal in 1 g of the catalyst forming 8-nm particles
10% of the metal in 1 g of the catalyst forming 12-nm particles.

Therefore, the average particle size as determined by TEM is:

$$\frac{1}{\bar{d}} = \frac{0.4}{3} + \frac{0.2}{5} + \frac{0.3}{8} + \frac{0.1}{12}$$

$$\bar{d} = 4.7 \text{ nm}.$$

If this catalyst had been examined by XPS, the standardized intensity ratio, N, obtained from the observed XPS dispersed phase/carrier intensity ratio would have the following value:

$$N = 0.4(N_3) + 0.2(N_5) + 0.3(N_8) + 0.1(N_{12}) = 0.576$$

where N_3, N_5, N_8, and N_{12} are the values of N in Fig. 4 at the corresponding particle dimensions. In order to use Fig. 4 to obtain a size measurement of the supported Pt particles from the observed XPS dispersed phase/carrier intensity ratio, we assume all the Pt particles are of the same size. From Fig. 4, Pt particles are determined to be 5.1 nm when $N = 0.576$. Therefore, the Pt particle size as determined by XPS is about 11% greater than that obtained by TEM under the above specified conditions. This overestimation signifies the large particles are weighted in favor over the small ones in arriving at the average particle size from XPS measurements. This is because X-ray photoelectron spectroscopy gives something between a surface and volume average size whereas TEM measurements result a surface average size.

ACKNOWLEDGMENTS

The author would like to thank Dr. R. T. K. Baker for providing the platinum sample, Dr. L. L. Murrell for providing the γ-Al_2O_3 supported tungsten catalysts, and Dr. J. H. Sinfelt for his helpful suggestions in preparing this article.

REFERENCES

1. Brinen, J. S., Schmitt, J. L., Doughman, W. R., Achorn, P. J., Siegel, L. A., and Delgass, W. N., *J. Catal.* **40**, 295 (1975).
2. Tomita, A., and Tamai, Y., *J. Catal.* **27**, 293 (1972).
3. Scharpen, L. H., *J. Electron Spectrosc.* **5**, 369 (1974).
4. Angevine, J. P., Delgass, W. N., and Vartuli, J. C., *Proc. Sixth Int. Congr. Catal.* **2**, 611 (1976).
5. Lindau, I., and Spicer, W. E., *J. Electron Spectrosc.* **3**, 409 (1974).
6. Biloen, P., and Pott, G. T., *J. Catal.* **30**, 169 (1973).
7. Ng, T. K., and Hercules, D. M., *J. Phys. Chem.* **80**, 2094 (1976).
8. DeBoer, J. H., Fahim, R. B., Linsen B. G., Visseren, W. J., and DeVleesschauwer, W. F. N. M., *J. Catal.* **7**, 163 (1967).
9. Carlson, T. A., and McGuire, G. E., *J. Electron Spectrosc.* **1**, 161 (1972/1973).
10. Baker, R. T. K., Prestridge, E. B., and Garten, R. L., *J. Catal.* **56**, 390 (1979).